Materials Research Proceedings 41 (2024) 1527-1535 https://doi.org/10.21741/9781644903131-169

Strain rates in high velocity forming of foils

LANGSTÄDTLER Lasse[1,2,3,a*], BECKSCHWARTE Björn[1,2,b], VALENTINO Tobias[4,c] and RADEL Tim[4,d]

[1]University of Bremen, Bibliothekstraße 1, 28359 Bremen, Germany

[2]BIME - Bremen Institute for Mechanical Engineering, Badgasteiner Straße 1, 28359 Bremen, Germany

[3]MAPEX - Center for Materials and Processes, 28334 Bremen, Germany

[4]BIAS - Bremer Institut für angew. Strahltechnik GmbH, Klagenfurter Str. 5, 28359 Bremen, Germany

[a]langstaedtler@bime.de, [b]beckschwarte@bime.de, [c]mikrofertigung@bias.de, [d]radel@bias.de

Keywords: Forming, In-Process Measurement, Electromagnetic Forming, Laser Shock Forming

Abstract. Energy- and working media based high velocity forming processes show various advantages forming metal foils. However, due to different process characteristics, differences in workpiece response by impulse transfer for different high velocity forming processes are expected. Free forming experiments with 50 µm metallic foils were carried out to identify the process influence, using electromagnetic forming and laser shock forming. For these two forming methods the response of the workpiece was described. The description was done by in-situ measurement of the strain and the strain rate over time and determination of workpiece velocities.

Introduction

High velocity forming technologies show the ability for shaping complex parts. Therefore, they are a key means of reducing a component's weight. Förster described in 1883 the advantages of high velocity forming. He used the detonation of explosives over a stamping die for engraving metal sheets [1]. Starting from these early experiments, further process advantages could be identified. Thus, the high forming velocity was described to increase formability of various materials [2]. Further, it was shown that the formation of winkles [3] and springback [4] is reducible due to high strain rates. In addition to these advantages, using inertial locking mechanisms in the design of the tools allows the use of smaller and therefore less expensive equipment [5]. High velocity forming was tested in a wide variety of objectives, workpieces and geometries to be produced around these processes. One field was the forming of thin foils, which brings with them the fundamental challenges of micro forming [6]. Energy- and working media-based high velocity forming processes enable to overcome these challenges.

One possibility to obtain is laser shock forming (LSF). The high repetition rate of lasers and the rapidly expanding shock wave offers the possibility of mass production of micro parts. Different laser-based high velocity forming process variants, such as deep drawing, bending, stretch drawing, and joining with a TEA-CO2-laser have been studied [7].

A further way of foil processing is electromagnetic forming (EMF). Here, volume dependent electromagnetic forces act onto the foils to be processed, whereby solutions for production and integration into the process chain already exist [8]. Different process variants of electromagnetic forming such as forming [9], embossing [10], cutting [11] and joining [12] metal foils were investigated.

The primary difference between the two forming techniques, which are capable to forming metal foils, is the difference in the energy transmission to the workpiece. During laser shock forming laser radiation causes thermo- and field emission of electrons, which irradiate out of the target surface. Collision processes between these highly energetic electrons and the atmosphere molecules produce ions. They absorb the ongoing laser radiation. Miziolek et al. described that these free ions absorb energy on the principle of inverse bremsstrahlung [13]. This sets an avalanche ionization in motion, which leads to plasma and subsequently, to shock wave formation and pressure increase, which is responsible for the forming of the foils. The expansion of the shock wave and therefore the pressure distribution can be influenced e.g., by pressure cells [14]. In contrast, in electromagnetic forming, forces are applied by the interaction of the workpiece with an electromagnetic field introduced by a transient current through a tool coil. Based on the penetration depth of the electromagnetic field and the sheet thickness, volume forces occur in the workpiece [15]. These volume forces and their distribution are directly related to the current density distribution and time series in the tool coil as well as in the workpiece. Further for insufficient shielding of the electromagnetic field by the thin workpiece, the inducted current in the surrounding parts can influence the workpiece during electromagnetic forming [16].

Both processes promote the advantages of high velocity forming for foils, but produce different energy transfer to the workpiece. The fundamental difference is the transient action of pressure in laser shock forming compared to the transient volume force in electromagnetic forming. Within this work the process effect on foil displacement was investigated experimentally. The resulting strain and strain rates over time were determined on the base of a free forming experiments and compared between both forming methods. Furthermore, reached velocities of the foils were calculated.

Materials and Methods

To investigate the impact of the impulse transfer during high velocity forming of thin foils, a free forming operation was used. Foils of Al99.5 (EN AW-1050), cut to a 50×50 mm² sheet, with a thickness s_0 of 50 µm were used as workpiece. The milled die was made of 90MnCrV8 as shown in Fig. 1 (a). The free forming operation was based on a rectangular cut-out of 8×16 mm² within the die. Furthermore, the cut-out was rounded with a 3 mm radius. For better accessibility, a cut-out was made on the unused die side. The installation of the die depended on the specific boundary conditions of the used forming processes. For the benefit of comparability, no distance between the workpiece and the die was used, so that the workpiece was in full contact with the die. Specific to the installation in electromagnetic forming was the contact of the tool coils 195 µm thick polyimide insulation with the workpiece (see Fig. 1 (b)). To avoid the influence of air, an additional gap of 135 µm in the middle section between the insulation and the workpiece was set. In the case of laser shock forming, on the other hand, a round blank holder with a diameter of 15 mm was used, which simultaneously defined the maximum effective area of the TEA-CO2 laser (see Fig. 1 (c)).

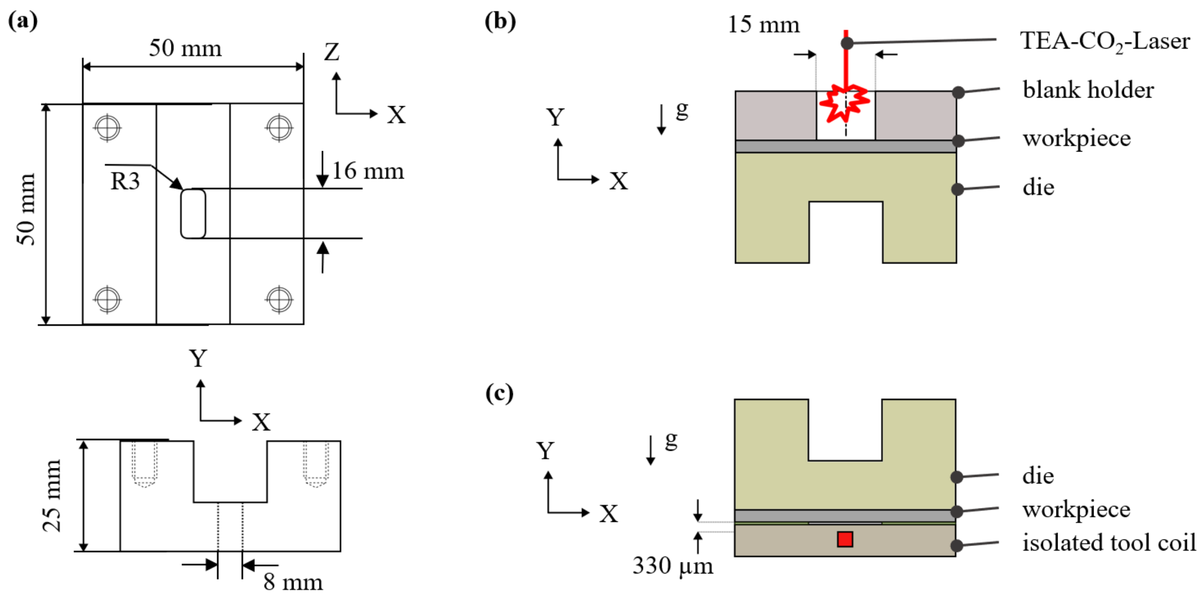

Fig. 1: Die geometry and installation: (a) sketch of the die geometry, (b) installation for LSF, (c) installation for EMF

The experiments were conducted with a TEA-CO2 laser (TEA = Transverse Excitation at Atmospheric Pressure). The pulse energy EP was emitted with a wavelength of λ of 10.6 µm with a pulse duration of t_p of 100 ns. The pulse duration refers to the full width at half maximum. The beam quality factor was M^2 of 28.4 and the spatial energy distribution was best approximated as homogeneous (flat-top). The pulse energy EP was set to 4.5 J. The laser beam was focused on a sheet via a concave focusing mirror with a focal length f of 200 mm. The focus was shifted 30 mm below the surface, resulting in a beam area of AF of 32 mm² on the sheet. A frequency of 50 Hz was used in the experiments with double pulse. Hence, the forming process of the first pulse was fully finished before the second starts. Further details about the basic laser system can be taken from Valentino [17].

Electromagnetic forming experiments were carried out with a pulsed power generator (see Fig. 2 (a)) with a total capacitor capacity C of 100 µF. During experiments a charge voltage U_0 of 2.82 kV and 4 kV was used, which results in a charge energy E_C of 800 J. Besides single discharges, multiple discharges were performed without changing the workpiece. As tool coil a single-conductor made of copper with a cross-section of 5×5 mm² was used (see Fig. 1 (c)). The charge energy E_C was switched by an ignitron (NL8900, National Electronics, LaFox, Il, USA), and resulted in a ≈ 700 µs long current oscillation with an oscillation frequency f_0 of ≈10 kHz (see Fig. 2 (b)). As a result of the resistances R_m, R_{tc} and R_c and inductances L_m, L_{tc} and L_c of the pulsed power generator, the tool coil current I_{tc} shown in Fig. 2 (b) was generated.

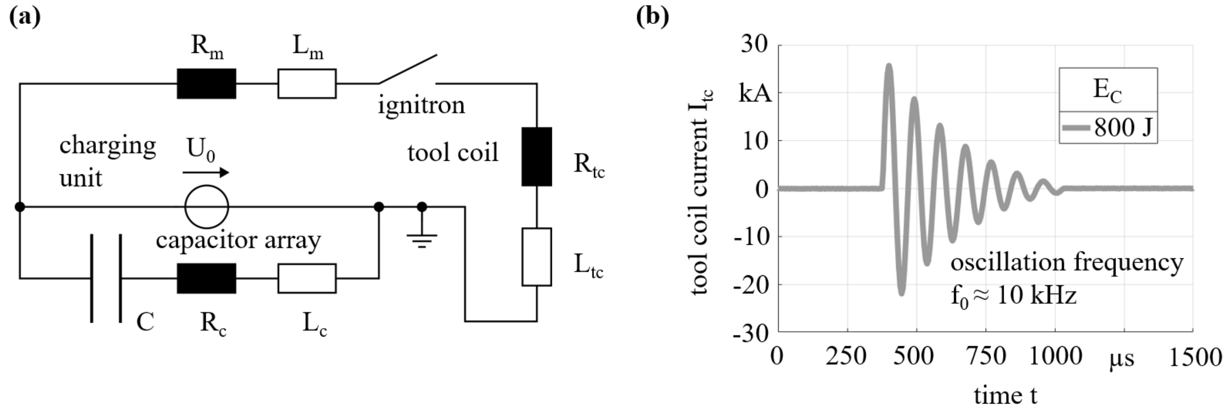

Fig. 2: Electromagnetic forming setup: (a) simplified electric circuit diagram, (b) resulting tool coil current I_{tc} over time t

A photoelectric sensor (LK-H157, Keyence, Osaka, Japan) was used to observe the displacement h of the workpiece sampled every 2.55 µs (see Fig. 3 (c)). The sensor was installed in the centre of the formed geometry (see Fig. 3 (a)) and its laser line was aligned transverse to the rolling orientation of the foils.

The resulting signal of the displacement h was filtered with a low-pass filter of 50 kHz. In connection with the circular shape in the X-Y-plane (see Fig. 3 (b)), the length of the arc segment L_1 was calculated from the displacement h (see Eq. 1).

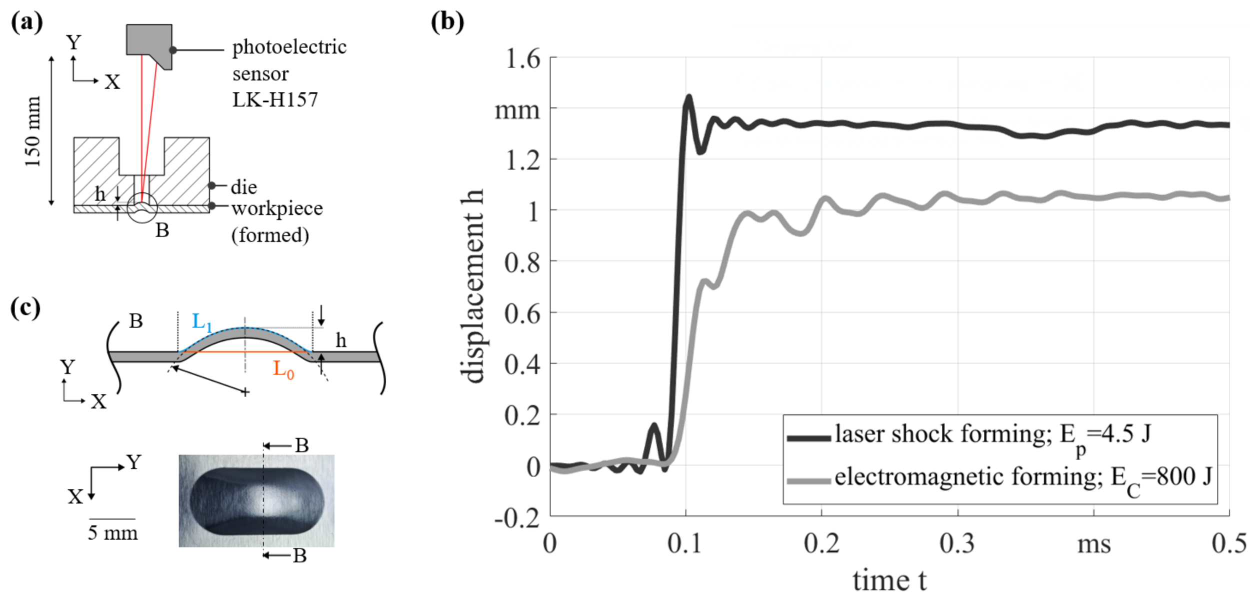

Fig. 3: Strain measurement: (a) sketch of the setup, (b) displacement h over time and (c) strain calculation

To calculate the strain over the formed geometry ε_g, the length L_1 was set in relation to the initial length L_0 (see Eq. 2). Further, the strain rate $\dot{\varepsilon}_g$ was determined by differentiate the strain ε_g over time t (see Eq. 3).

$$L_1 = \frac{\tan^{-1}\frac{2*h}{L_0} * \left(4*h^2 + {L_0}^2\right)}{2*h} \tag{1}$$

$$\varepsilon_g = \frac{L_1 - L_0}{L_0} \tag{2}$$

$$\dot{\varepsilon}_g = \frac{\Delta\varepsilon_g}{\Delta t} \tag{3}$$

For comparison of the measuring system used, the deformation velocity v_d was calculated according to Veenas et al. [7]. Furthermore, the present workpiece velocity v_w hence the maximum workpiece velocity $v_{w,m}$ was obtained by derivation of the displacement h (see Eq. 4).

$$v_w = \frac{\Delta h}{\Delta t} \tag{4}$$

Results

Fig. 4 compares the measured average velocity with the results determined by Veenaas et al. [7]. Minor differences were expected in this comparison due to the deviation of the die geometry, Fig. 4 (a). The results determined with the position sensor were comparable with the ones determined via the light barrier by Veenaas et al, which validated the suitability of the position sensor in high velocity foil forming, Fig. 4 (b). Based on the definition of the deformation velocity v_d, there was found a deviation to the present workpiece velocity v_w. Fig. 4 (c) shows the maximum reached workpiece velocity $v_{w,m}$.

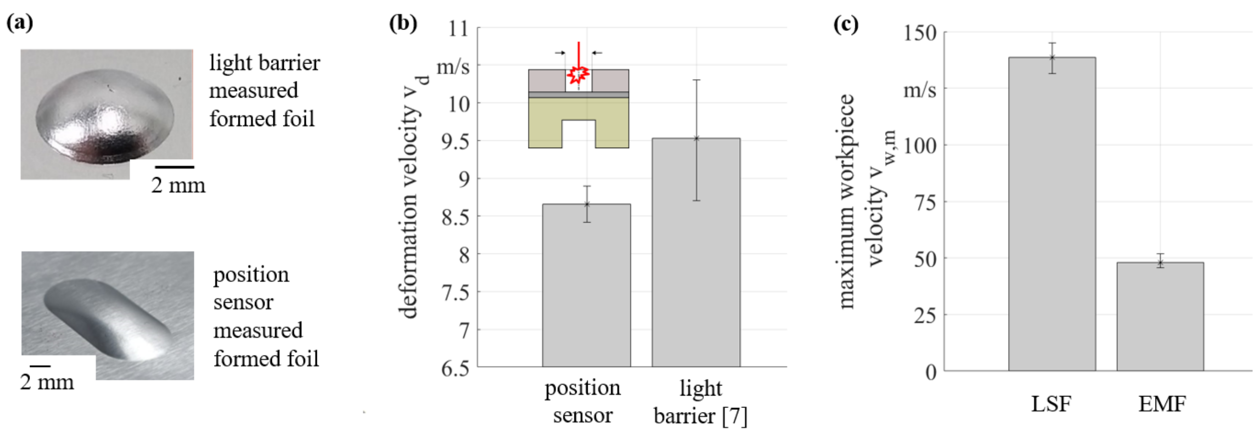

Fig. 4: Measurement system: (a) formed foils for different tests methods, (b) comparison of measured velocities v_d for position sensor and light barrier, (c) workpiece velocities $v_{w,m}$ determined for LSF and EMF

Higher maximum workpiece velocity $v_{w,m}$ were measured - using the current settings - for laser shock forming compared to electromagnetic forming. Nevertheless, both processes exceed the workpiece velocity limit of 15 m/s for high velocity forming processes defined by Bruno et al. [18].

In laser shock forming, three phases of forming were identified (see Fig. 5). The first phase preceded the actual forming, where a small alternating strain ε_g occurred. This phase could be a result of the plasma initiation. After this phase, the main deformation occurred up to the maximum of the strain. Here, a strain rate $\dot{\varepsilon}_g$ of 10000 1/s was calculated based on the displacement measurement (see Fig. 5 (b)). Following this phase, a phase of springback of the workpiece arose, which ended with a remaining strain of approx. 0.074 (see Fig. 5 (a)). After this, a variation in strain and strain rate was determined due to the process-induced vibration and noise of the measurement system.

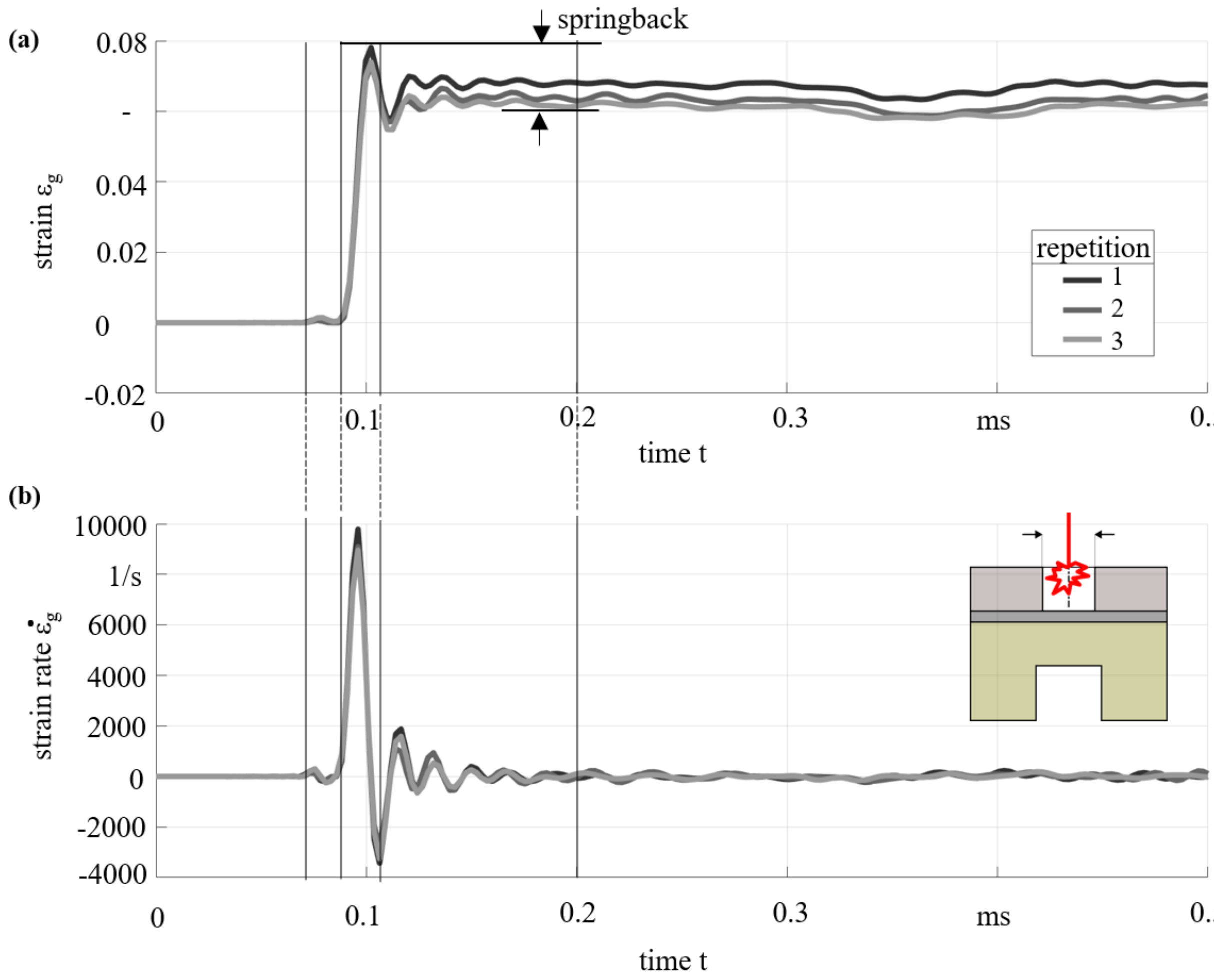

Fig. 5: Laser shock forming: (a) strain ε_g over time t, (b) strain rate $\dot{\varepsilon}_g$ over time t

Free electromagnetic forming could be divided into two phases (see Fig. 6). The first phase consisted of the elongation of the workpiece up to the first reach of the remaining strain ε_g.

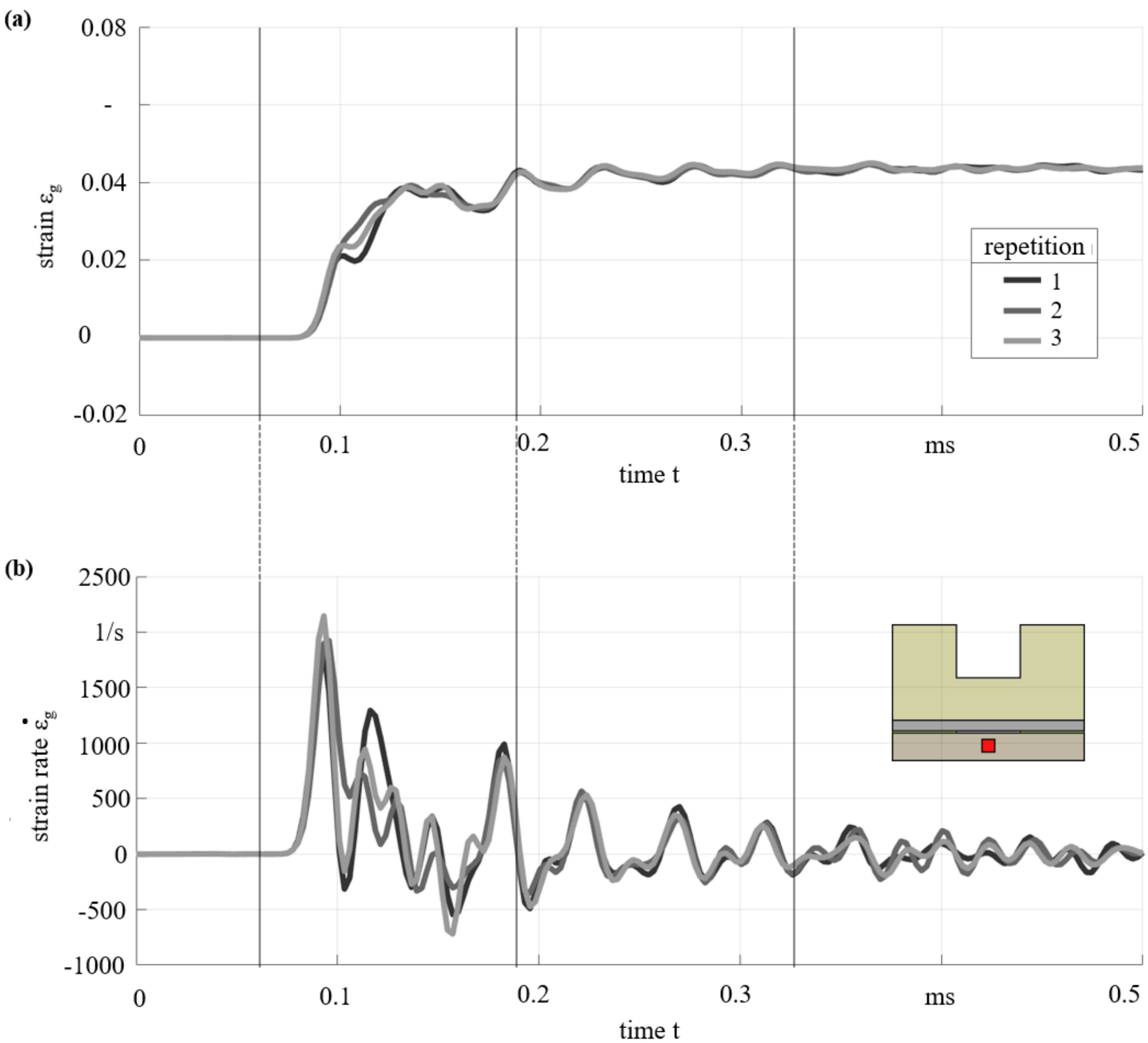

Fig. 6: Electromagnetic forming; (a) strain ε_g over time t (b) strain rate $\dot{\varepsilon}_g$ over time t

Based on the oscillation of the electromagnetic force indicated by the oscillation of the tool coil current I_{tc}, a discontinuous straining takes place. Within this phase, the highest strain rate $\dot{\varepsilon}_g$ of approx. 2100 1/s occurred (see Fig. 6 (b)). Following to this phase, a workpiece vibration around the remaining strain ε_g arose with a maximum strain rate $\dot{\varepsilon}_g$ of approx. 1000 1/s with no springback. As the amplitude of the workpiece vibration decays, a strain ε_g of approx. 0.044 remained. Again, due to the vibration of the measuring system and noise, a variation of the strain ε_g and strain rate $\dot{\varepsilon}_g$ appeared.

Discussion

Both forming processes fulfil the high-velocity criteria established by Bruno et al. [18]. Nevertheless, both differ in their process effect, so that different characteristics occurred during the forming process. During laser shock forming, a surface force acted which had its origin above the surface. On the other hand, volume forces acted during electromagnetic forming. As a result of the different force application, different time sequences of the forming occurred. As a reaction to the pressure wave during laser shock forming, a single movement occurred. The actual forming motion was preceded by a workpiece motion, which could be a result of the plasma or shockwave initiation. In electromagnetic forming, a movement occurred as a function of the tool coil current, which was divided into the actual forming and vibration for the tool coil current used [19].

Conclusion

A new measurement set up for investigation of different high velocity forming processes was introduced in this paper. The comparison with a light barrier-based measurement system showed the useability as well as advantages of the new system for investigation of energy transmission in high velocity forming processes.

Based on the first experiments comparing laser shock forming and electromagnetic forming with 50 µm thin Al99.5 foils following conclusion can be drawn:

- LSF and EMF are characterized as high-speed forming processes with maximum workpiece velocity over 15 m/s
- The reached maximum velocity of LSF ≈135 m/s was higher than for EMF with ≈50 m/s
- Differences in strain and strain rate over time were observed
- EMF showed reduction of springback which was explained by force oscillation

Future work

The method used made it possible to determine the deformation at one point on the sheet metal. Since impulse forming processes such as electrohydraulic forming are based on the effect of transient pressure fields, the aim is to extend the method for future investigations of energy transfer, e.g. by adding further distance sensors and pressure sensors in the pressure-transmitting fluid.

References

[1] D.R. Kennedy, History of the shaped charge effect: The first 100 years, (1983).

[2] G. Avrillaud et al., Examples of How Increased Formability through High Strain Rates Can Be Used in Electro-Hydraulic Forming and Electromagnetic Forming Industrial Applications, J. of Man. and Mat. Pro. 5 (3), (2021) 96. https://doi.org/10.3390/jmmp5030096

[3] H.-G. Noh et al., Two-step electromagnetic forming process using spiral forming coils to deform sheet metal in a middle-block die, Int J Adv Man. Technol., 76 (9-12), (2015) 1691-1703. https://doi.org/10.1007/s00170-014-6392-4

[4] X. Cui et al., Springback Calibration of a U-Shaped Electromagnetic Impulse Forming Process, Metals 9 (5) 603. https://doi.org/10.3390/met9050603

[5] Z Lai et al., Application of Electromagnetic Forming as a Light-Weight Manufacturing Method for Large-Scale Sheet Metal Parts, (2018).

[6] M. Geiger et al., Microforming, CIRP Annals 50 (2), (2001) 445-462. https://doi.org/10.1016/S0007-8506(07)62991-6

[7] S. Veenaas et al., Determination of forming speed at a laser shock stretch drawing process, Proceedings of the 7th ICHSF, (2016) 105-114.

[8] B. Kuhfuss et al., Electromagnetic Linked Micro Parts Processing, Proc. Eng. 81, (2014) 2135-2140. https://doi.org/10.1016/j.proeng.2014.10.298

[9] Z. Long et al., Electromagnetic micro-forming using flat spiral coil, Int. J. Adv. Manuf. Technol. 121 (1-2), (2022) 1161-1171. https://doi.org/10.1007/s00170-022-09363-1

[10] Z. Zimniak, Plastic Deformation Zone in Electromagnetic Cutting, Archives of Metallurgy and Materials 62 (4), (2017) 2303-2308. https://doi.org/10.1515/amm-2017-0339

[11] M. Kamal et al., Agile manufacturing of a micro-embossed case by a two-step electromagnetic forming process, J. of Mat. Pro. Tec. 190, (2007) 41-50. https://doi.org/10.1016/j.jmatprotec.2007.03.114

[12] L. Langstädtler et al., Electromagnetic Joining of Thin Sheets by Adapted Pulses, KEM 767, (2018) 439-446. https://doi.org/10.4028/www.scientific.net/KEM.767.439

[13] A. W. Miziolek et al., Laser Induced Breakdown Spectroscopy, Cambridge University Press, (2006). https://doi.org/10.1017/CBO9780511541261

[14] H. Fenske et al., Tailoring the Pressure Profile of TEA-CO2 Laser-Induced Shock Waves for Mechanical Forming and Separation Processes, Lasers Manuf. Mater. Process. 7 (1), (2020) 1-14. https://doi.org/10.1007/s40516-019-00105-y

[15] H. Bühler et al., Ein Beitrag zur Magnetumformung rohrförmiger Werkstücke, Werkstatt und Betrieb 110.9, (1968) 513-516.

[16] B. Beckschwarte et al., Numerical and Experimental Investigation of the Impact of the Electromagnetic Properties of the Die Materials in Electromagnetic Forming of Thin Sheet Metal, J. manuf. mater. process. 5 (1), (2021) 18ff. https://doi.org/10.3390/jmmp5010018

[17] T. Valentino, Nutzung laserinduzierter Stoßwellen zur Hochdurchsatz-Werkstoffprüfung, (2021).

[18] E. J. Bruno, High-velocity forming of metals, American Society of Tool and Manufacturing Engineers, (1968).

[19] B. Beckschwarte et al., Response of Thin Sheet Metal on the Excitation in Electromagnetic Forming, Eng. Proc. 26 (1), (2022) 4. https://doi.org/10.3390/engproc2022026004